The Thermal Decomposition of Water

N. K. SRINIVASAN, J. V. MICHAEL

Chemistry Division, Argonne National Laboratory, Argonne, IL 60439

Received 5 July 2005; revised 18 October 2005; accepted 26 October 2005

DOI 10.1002/kin.20172
Published online in Wiley InterScience (www.interscience.wiley.com).

ABSTRACT: The reflected shock tube technique with multipass absorption spectrometric detection of OH-radicals at 308 nm, corresponding to a total path length of 1.749 m, has been used to study the reaction $H_2O + M \rightarrow H + OH + M$ between 2196 and 2792 K using 0.3, 0.5, and 1% H_2O, diluted in Kr. As a result of the increased sensitivity for OH-radical detection, the existing database for this reaction could be extended downward by ~500 K. Combining the present work with that of Homer and Hurle, the composite rate expression for water dissociation in either Ar or Kr bath gas is $k_{1,\mathrm{Ar(or\,Kr)}} = (2.43 \pm 0.57) \times 10^{-10} \exp(-47117 \pm 633\ K/T)$ cm^3 molecule^{-1} s^{-1} over the T-range of 2196–3290 K. Applying the Troe factorization method to data for both forward and reverse reactions, the rate behavior could be expressed to within <±18% over the T-range, 300–3400 K, by the three-parameter expression $k_{1,\mathrm{Ar}} = 1.007 \times 10^4\ T^{-3.322} \exp(-60782\ K/T)$ cm^3 molecule^{-1} s^{-1} A large enhancement due to H_2O with H_2O collisional activation has been noted previously, and both absolute and relative data have been considered allowing us to suggest $k_{1,\mathrm{H_2O}} = 1.671 \times 10^2\ T^{-2.440} \exp(-60475\ K/T)$ cm^3 molecule^{-1} s^{-1} for the rate constants with H_2O bath gas over the T-range, 300–3400 K. © 2006 Wiley Periodicals, Inc. Int J Chem Kinet 38: 211–219, 2006

INTRODUCTION

Because it is important in H_2/O_2 flame chemistry, the thermal decomposition of H_2O

$$H_2O + M \rightarrow OH + H + M \qquad (1)$$

has been studied five times [1–5]. The direct studies, either by observing H_2O depletion [2,4] or by OH-radical formation [1–3], have been confined to relatively large $[H_2O]_0$ at temperatures above ~2700 K because the sensitivity for detection has been relatively low. We have recently described a multipass optical system that allows for the detection of OH-radicals in concentrations between $\sim 2 \times 10^{12}$ and 2×10^{14} molecules cm^{-3} [6]. Hence, rate constants can be measured at lower temperatures, and this study now extends the H_2O decomposition database to 500 K below the previous studies and allows for determinations of the equally important rate constants for the reverse reaction, $k_{-1,\mathrm{M}}$.

EXPERIMENTAL

The present experiments were performed with the shock tube technique using OH-radical electronic absorption detection. The method and the apparatus

Correspondence to: J. V. Michael; e-mail: jmichael@anl.gov.

Contract grant sponsor: Office of Basic Energy Sciences, Division of Chemical Sciences, Geosciences, and Biosciences, U.S. Department of Energy.

Contract grant number: W-31-109-Eng-38.

currently being used have been previously described [7,8], and only a brief description of the experiment will be presented here.

The shock tube is constructed from 304 stainless steel in three sections. The first 10.2 cm-o.d. cylindrical section is separated from the He driver chamber by a 4-mil unscored 1100-H18 aluminum diaphragm. A 0.25-m transition section then connects the first and third sections. The third section is of rounded corner (radius, 1.71 cm) square design and is fabricated from flat stock (3 mm) with a mirror finish. Two flat fused silica windows (3.81 cm) with broadband antireflection (BB AR) coating for UV light are mounted on the tube across from one another at a distance of 6 cm from the end plate. The path length between windows is 8.745 cm. The incident shock velocity is measured with eight fast pressure transducers (PCB Piezotronics, Inc., model 113A21) mounted along the third portion of the shock tube, and temperature and density in the reflected shock wave regime are calculated from this velocity and include corrections for boundary layer perturbations [9–11]. The tube is routinely pumped between experiments to $<10^{-8}$ Torr by an Edwards Vacuum Products model CR100P packaged pumping system. A 4094C Nicolet digital oscilloscope was used to record both the velocity and absorption signals.

The optical configuration consists of an OH resonance lamp, multipass reflectors, an interference filter at 308 nm, and a photomultiplier tube (1P28), all mounted external to the shock tube as described previously [6,12–14]. With this new configuration, a total path length of 1.749 m was obtainable, thereby amplifying the measured absorbances by 20.

Gases

High purity He (99.995%), used as the driver gas, was obtained from AGA Gases. Scientific grade Kr (99.999%), the diluent gas in reactant mixtures, was obtained from Spectra Gases, Inc. The ~10 ppm impurities (N_2—2 ppm, O_2—0.5 ppm, Ar—2 ppm, CO_2—0.5 ppm, H_2—0.5 ppm, CH_4—0.5 ppm, H_2O—0.5 ppm, Xe—5 ppm, and CF_4—0.5 ppm) are all either inert or in sufficiently low concentration so as to not perturb OH-radical profiles. Distilled water, evaporated at 1 atm into ultra-high purity grade Ar (99.999%) from AGA Gases, was used at ~25 Torr pressure in the resonance lamp. The water used as reactant was triple distilled and was additionally purified by bulb-to-bulb distillation in the vacuum line with the middle third being retained. Test gas mixtures were accurately prepared from pressure measurements using a Baratron capacitance manometer and were stored in an all glass vacuum line.

RESULTS

Thirty-eight experiments were performed to investigate the thermal decomposition of H_2O in the reflected shock wave regime over the T-range, 2200–2800 K, using three reaction mixtures, 0.3, 0.5, and 1% H_2O, diluted in Kr. The experimental conditions and the results are summarized in Table I. The temporal concentration buildup of the product, $[OH]_t$, was determined from measured absorbance, $ABS_t = \ln[I_0/I_t] = [OH]_t \ell \sigma_{OH}$, through an earlier determination of the absorption cross-section at 308 nm [6].

Figure 1 shows two typical [OH] profiles at two different temperatures, 2367 and 2588 K, respectively. The thick solid lines are fits from a chemical simulation using the nine-step reaction mechanism of Table II, but varying only the rate of reaction (1). All other reactions listed in the table are taken from the literature and are known sufficiently well that they cannot be varied in the fitting procedure. For the profiles shown in Fig. 1 and other lower-T experiments ($T < 2600$ K), varying the rate of reaction (1) gives excellent fits when extended to 1.2 ms. It is not surprising that at low-T and low $[H_2O]_0$, secondary bimolecular atom-transfer reactions are far too slow to affect the experimental profiles since the product concentrations (i.e., H, OH, and O) are low and cannot compete with the rate of dissociation of the parent molecule. Hence, the present reaction (1) rate constants for the $T < 2600$ K experiments listed in Table I are unambiguously direct.

In order to inhibit the effects of secondary reactions at higher-T, experiments at $T > 2700$ K were conducted with very dilute (0.3% H_2O in Kr) mixtures. As pointed out in the earlier studies [1–5], the only other reaction that is fast and contributes to the OH formation rates at early times is $H + H_2O \rightarrow OH + H_2$ (reaction (2) in Table II). As shown in Fig. 2 in a chemical simulation at 2712 K with reaction (2) taken to be zero, a ~50% decrease in the simulated $[OH]_t$ is predicted (long dashed line). However, a 50% increase in k_2 results in <2% increase in $[OH]_t$ even at later times (~1.2 ms) as also shown in Fig. 2 (short dashed line compared to the thick solid line). As seen in the 2712 K experimental profile shown in the figure, the signal-to-noise ratio is low primarily due to our decision to work with low $[OH]_0$ and high sensitivity (20 optical passes). Hence, it is important to determine the uncertainty in the final values of $k_{1,M}$ listed in Table I. Changing the value of $k_{1,M}$ that best fits the profile in the figure by ±20% results in fits that are either too low or too high as shown by the thin solid lines. A linear sensitivity analysis is shown in Fig. 3 for the profile of Fig. 2 using the final fitted

Table I High Temperature Rate Data for $H_2O + M \rightarrow H + OH + M$

P_1/(Torr)	M_s[a]	$\rho_5/(10^{18}$ cm$^{-3})$[b]	T_5/(K)[b]	$k_{1,M}$
		$X_{H_2O} = 2.972 \times 10^{-3}$		
5.98	3.105	1.366	2345	9.48(−19)[c]
5.96	3.274	1.408	2600	2.16(−18)
5.97	3.213	1.392	2510	1.46(−18)
5.94	3.168	1.381	2428	1.02(−18)
5.93	3.271	1.404	2588	2.75(−18)
5.88	3.401	1.425	2792	5.59(−18)
5.95	3.353	1.431	2712	3.60(−18)
5.95	3.433	1.424	2706	7.66(−18)
5.96	3.255	1.408	2572	2.42(−18)
5.91	3.203	1.375	2496	1.48(−18)
10.92	3.145	2.509	2382	6.73(−19)
10.98	3.268	2.589	2559	2.37(−18)
10.95	3.096	2.488	2311	2.72(−19)
10.96	3.265	2.583	2555	1.57(−18)
10.94	3.042	2.455	2237	1.92(−19)
10.94	3.263	2.577	2553	1.31(−18)
10.92	3.192	2.535	2448	1.47(−18)
10.89	3.275	2.572	2571	2.07(−18)
		$X_{H_2O} = 1.001 \times 10^{-2}$		
5.91	3.330	1.420	2668	3.77(−18)
5.98	3.244	1.413	2539	2.55(−18)
5.97	3.185	1.389	2460	1.36(−18)
5.99	3.045	1.349	2261	3.27(−19)
5.94	3.190	1.383	2468	1.31(−18)
5.95	3.126	1.370	2367	1.05(−18)
5.92	3.277	1.408	2588	2.91(−18)
5.92	3.160	1.374	2414	1.44(−18)
5.94	3.237	1.401	2529	1.71(−18)
5.95	3.124	1.370	2364	6.25(−19)
		$X_{H_2O} = 5.011 \times 10^{-3}$		
10.93	3.113	2.494	2335	4.73(−19)
10.94	3.039	2.453	2232	2.12(−19)
10.90	3.261	2.567	2550	2.03(−18)
10.89	3.012	2.426	2196	2.05(−19)
10.98	3.323	2.618	2642	3.10(−18)
10.94	3.153	2.518	2393	5.93(−19)
10.95	3.148	2.518	2385	4.98(−19)
10.97	3.403	2.646	2774	5.87(−18)
10.95	3.198	2.527	2466	1.72(−18)
10.91	3.131	2.491	2369	4.17(−19)

[a] The error in measuring the Mach number, M_s, is typically 0.5–1.0% at the one standard deviation level.
[b] Quantities with the subscript 5 refer to the thermodynamic state of the gas in the reflected shock region.
[c] Parentheses denote the power of 10.

value for $k_{1,M}$ with other reactions in the mechanism unchanged. It is clear that $H_2O + Kr \rightarrow H + OH + Kr$ is without question the dominant process over the entire 1.2 ms time range with negligible sensitivity from k_2 ($H + H_2O \rightarrow OH + H_2$). As pointed out before, this reaction is so fast that it does not affect our decision on $k_{1,M}$. Figure 4 shows an Arrhenius plot of the $k_{1,M}$ values in Table I over the entire temperature range, 2196–2792 K.

DISCUSSION

It is clear from earlier discussions that the results of Bauer et al. [1] were compromised by secondary

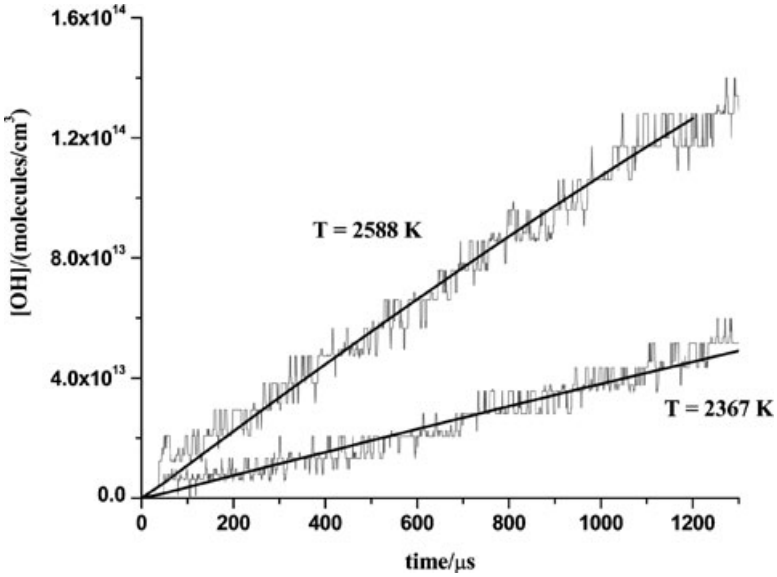

Figure 1 Measured OH-radical profiles for two typical experiments. Solid lines—fits with reaction mechanism listed in Table II. The conditions for the upper trace are $P_1 = 5.92$ Torr and $M_s = 3.277$, $T_5 = 2588$ K, $\rho_5 = 1.408 \times 10^{18}$ molecules cm^{-3}, and $[H_2O]_0 = 1.409 \times 10^{16}$ molecules cm^{-3}. The conditions for the lower trace are $P_1 = 5.95$ Torr and $M_s = 3.126$, $T_5 = 2367$ K, $\rho_5 = 1.370 \times 10^{18}$ molecules cm^{-3}, and $[H_2O]_0 = 1.371 \times 10^{16}$ molecules cm^{-3}.

reactions due to the large $[H_2O]_0$ necessary for detection of OH-radicals. Although Olschewski et al. [2] were able to use infrared emission of water at 2.8 μm to measure $[H_2O]_t$, their experiments, using optical absorption of OH, were not successful in measuring the dissociation rate constant, again probably due to secondary reactions. Bopp et al. [4] also used infrared emission to observe D_2O dissociation but made no attempt to estimate isotope effects. The experiments by Cathro and Mackie [5] contained ∼8–10% H_2O and relied on the assumption of equilibrium in the reaction, $Li + H_2O = LiOH + H$. Considering all previous studies, the experiments of Homer and Hurle [3] appear to be the most thorough even though the delayed flash

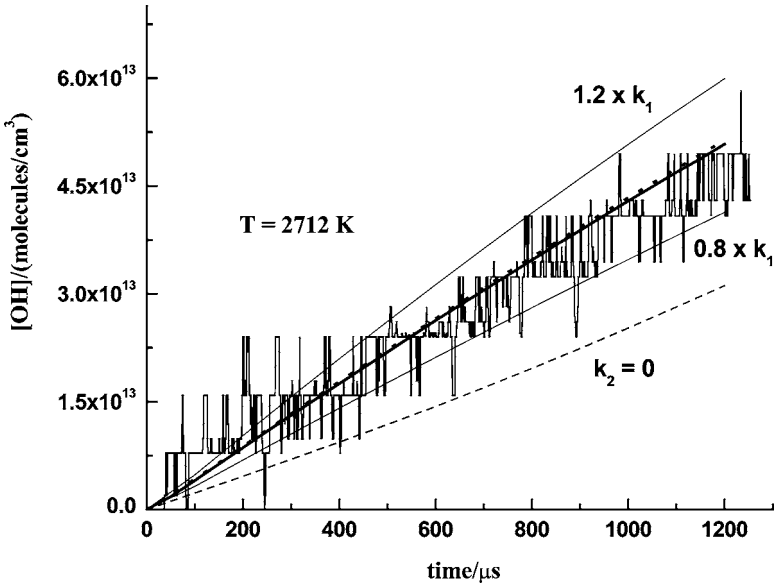

Figure 2 A temporal profile of OH absorption. Solid line—fits with full reaction mechanism listed in Table II. Dashed line—simulation with $k_2 = 0$. Thin solid lines and short-dashed line (see text). $P_1 = 5.95$ Torr and $M_s = 3.353$, $T_5 = 2712$ K, $\rho_5 = 1.431 \times 10^{18}$ molecules cm^{-3}, and $[H_2O]_0 = 4.253 \times 10^{15}$ molecules cm^{-3}.

Table II Mechanism for H_2O Dissociation

Reaction	Rate Constant[a]
1. $H_2O + Kr \rightarrow H + OH + Kr$	k_1 = to be fitted
2. $H + H_2O \rightarrow OH + H_2$	$k_2 = 1.56 \times 10^{-15}\ T^{1.52} \exp(-9083\ K/T)$
3. $OH + OH \rightarrow O + H_2O$	$k_3 = 7.19 \times 10^{-21}\ T^{2.7} \exp(917\ K/T)$
4. $O + H_2O \rightarrow OH + OH$	$k_4 = 7.48 \times 10^{-20}\ T^{2.7} \exp(-7323\ K/T)$
5. $H + O_2 \rightarrow OH + O$	$k_5 = 1.62 \times 10^{-10} \exp(-7474\ K/T)$
6. $OH + O \rightarrow O_2 + H$	$k_6 = 5.42 \times 10^{-13}\ T^{0.375} \exp(950\ K/T)$
7. $O + H_2 \rightarrow OH + H$	$k_7 = 8.44 \times 10^{-20}\ T^{2.67} \exp(-3167\ K/T)$
8. $OH + H \rightarrow H_2 + O$	$k_8 = 3.78 \times 10^{-20}\ T^{2.67} \exp(-2393\ K/T)$
9. $OH + H_2 \rightarrow H_2O + H$	$k_9 = 3.56 \times 10^{-16}\ T^{1.52} \exp(-1736\ K/T)$

[a] All rate constants are in cm^3 $molecule^{-1}$ s^{-1} from [15], modified with new OH heat of formation from [16].

absorption of OH required extraordinary control over shock strengths in successive experiments. These authors varied $[H_2O]/[Ar]$ by about a factor of 10 and directly documented a strong increase in the rate constant due to H_2O with H_2O collisional activation. At 2930 K, they report $k_{1,H_2O} = (20 \pm 7)k_{1,Ar}$. This enhancement was previously suggested in H_2/O_2 shock tube studies by Getzinger and Blair [17] who reviewed earlier studies documenting the effect. Such enhancement should occur with permanent dipole with dipole collisions as discussed recently in work from this laboratory on HO_2 with H_2O collisions [18].

If the previous studies are compared, the results of Homer and Hurle [3] are about a factor of 2 higher than both studies based on water depletion [2,4]. Taking into account the enhancement due to H_2O–H_2O collisions with the dilutions used in this work, the present results for $k_{1,M}$, given in Table I, will have only a 5–10% water contribution. This is well within the scatter of the data points, and, therefore, the present results refer to $k_{1,Kr}$, within experimental error.

$k_{1,Ar}$ can be determined from the data of Homer and Hurle [3] with the reasonable assumption that $k_{1,H_2O} = 20k_{1,Ar}$ over their entire T-range, 2570–3290 K. Then their $k_{1,Ar} = k_{1,M}([Ar] + [H_2O])/([Ar] + 20[H_2O])$ and their derived values (shown as crosses) are also plotted in Fig. 4, where good agreement is seen between the two sets of data. In dissociation or recombination studies, the collisional efficiency factors for Ar and Kr are generally equal to one another within experimental error, and we have therefore combined both to determine the temperature dependence of the rate constant, giving both sets equal statistical weight, obtaining

$$k_{1,Kr(or\ Ar)} = (2.43 \pm 0.57) \times 10^{-10} \exp(-47117 \pm 633K/T)\ cm^3\ molecule^{-1}\ s^{-1} \quad (2)$$

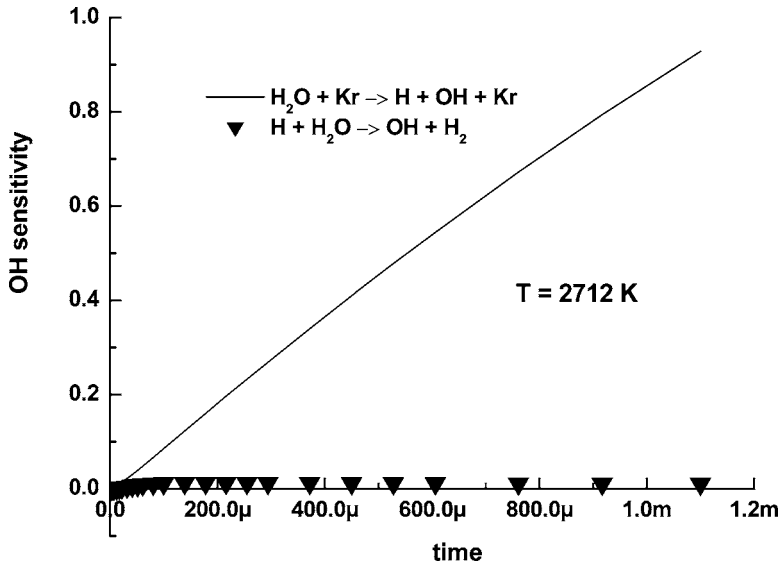

Figure 3 OH-radical sensitivity analysis for the 2712 K profile shown in Fig. 2 using the full reaction mechanism scheme and the final-fitted values for $k_{1,M}$. The two most sensitive reactions are shown.

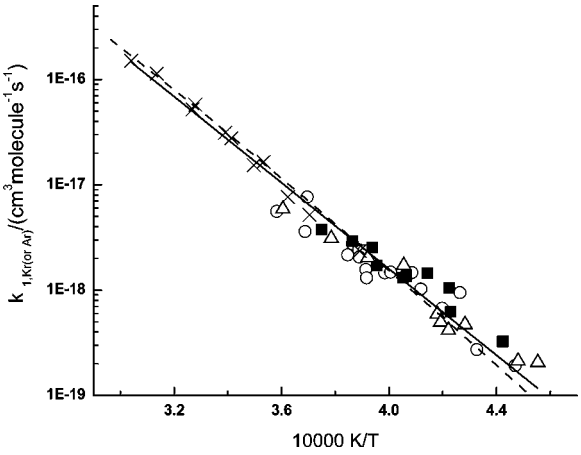

Figure 4 Arrhenius plot of the data for $k_{1,M}$ from Table I. (○)—present work (0.3% H_2O/Kr), (△)—present work (0.5% H_2O/Kr), (■)—present work (1% H_2O/Kr), and (X)—[3] (see text) Solid line—(Eq. (2) in text), and dashed line—(Eq. (4) in text).

over the temperature range, 2196–3290 K. The experimental data are within ±26% of Eq. (2), and the line determined from (2) is shown in Fig. 4 as the solid line.

The combined experimental result, Eq. (2), can be discussed in terms of the Troe factorization method [19], where the strong collision low-pressure bimolecular rate constant is given by

$$k_0^{sc} = Z_{LJ} F_{anh} F_{rot} F_E \left(\frac{\rho_{vib,h}(E_0) kT}{Q_{vib}} \right) \exp\left(\frac{-E_0}{kT} \right) \quad (3)$$

The various terms in Eq. (3) are evaluated and listed in Table III using the input values [16,20] given in the footnotes to the table. Except for minor changes in both E_0 [16] and the method for calculating Z_{LJ} [20], the calculations for k_0^{sc} duplicate those of Troe [19]. Application of the complete theory [21,22] shows that falloff effects are unimportant due to the small density of states at the threshold energy. Hence, the experimental rate determination, Eq. (2), refers to the low-pressure limit.

Between 2200 and 3400 K, collisional efficiency factors, $\beta_{c,exp}$ listed in Table III, were then determined by fitting values calculated from Eq. (2) to theory. Within ~±0.2%, the values of $\beta_{c,exp} \times k_0^{sc}$ reproduce Eq. (2) over the T-range, implying values for $\beta_{c,exp}$ between 0.052 and 0.012, in substantial agreement with Troe [19]. Zellner et al. [23] have carried out experiments on the reverse reaction, $k_{-1,M}$, near room temperature, and they have also applied Troe factorization to explain their results. For Ar bath gas, they report $k_{-1,Ar} = 2.3 \times 10^{-33}$ cm^6 molecule^{-2} s^{-1} at 300 K which yields $\beta_{c,exp} = 0.33$ using similar input values to those used here. Hence, collisional efficiency factors vary by ~28 from 300 to 3400 K.

In an attempt to specify intermediate temperature rate constant values, we have considered the Zellner et al. [23] work and four other approximate rate constant values for $k_{-1,Ar}$ from branched chain H_2 oxidation studies [17,24–26]. Since there is no viable method for a priori determination of β_c values, we have transformed Eq. (2) to $k_{-1,Ar}$ with the equilibrium constant given in the footnotes to Table III [16] and have carried out a second-order polynomial fit of these and other third-order values in Ar [17,23–26] in a $\log(k_{-1,Ar})$ against $\log(T)$ correlation. The resulting fit is shown in Fig. 5 as a solid line along with the data used to specify it. With this correlation, we then have determined a set of β_c values that smoothly joins the low- [23] and the present high-T transformed values, i.e., the transformed values from Eq. (2). These values are likewise listed in Table III as $\beta_{c,calc}$. It is worth noting that this set of β_cs cannot be used to specify sensible energy transfer parameters, i.e., ΔE_{down}'s. The implied ΔE_{down} values increase to a maximum and then monotonically decrease with increasing temperature. In any case, using $k_{1,Ar} = \beta_{c,calc} \times k_0^{sc}$, the dissociation rate constant can be represented by the three-parameter expression

$$k_{1,Ar} = 1.007 \times 10^4 \, T^{-3.312} \exp(-60782 \, K/T) \, \text{cm}^3 \, \text{molecule}^{-1} \, \text{s}^{-1} \quad (4)$$

to within <±18% over the T-range, 300–3400 K. Equation (4) is also plotted in Fig. 4 as the dashed line along with the high-T experimental results where it is seen to clearly describe the data within an estimated experimental error of ~ ±30%.

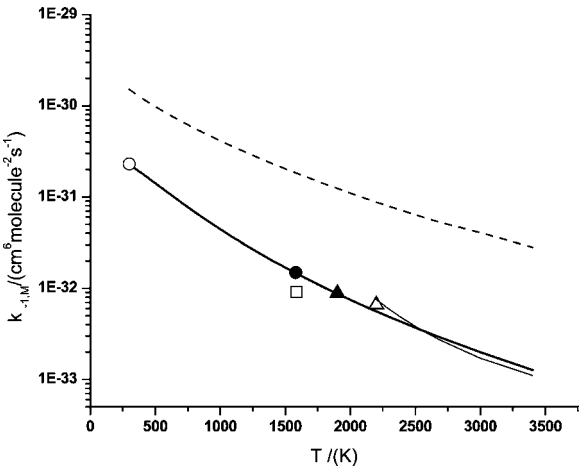

Figure 5 Plot of log $k_{-1,M}$ against T where (○)—[23], (●)—[24], (□)—[17], (▲)—[25], and (△)—[26]. Thick solid line—(see text), thin solid line—(Eq. (2) transformed using K_{eq}), and dashed line—(Eq. (5) transformed using K_{eq}) see text for details.

Table III Theory for $H_2O + Kr \rightarrow H + OH + Kr$[a–d]

T/(K)	F_{rot}	F_E	$Z_{LJ}/(10^{-10})$[e,f]	k_0^{sc}[f]	$\beta_{c,exp}$	$\beta_{c,calc}$
300	94.36	1.009	4.59	2.14(−92)[g]	0.33[h]	0.374[i]
400	82.46	1.012	4.31	6.15(−71)		0.369
500	73.09	1.015	4.24	4.75(−58)		0.333
600	65.43	1.018	4.25	1.88(−49)		0.292
700	59.03	1.022	4.30	2.60(−43)		0.252
800	53.60	1.025	4.38	1.05(−38)		0.216
900	48.93	1.028	4.46	3.98(−35)		0.186
1000	44.89	1.031	4.54	2.89(−32)		0.161
1100	41.36	1.034	4.63	6.30(−30)		0.139
1200	38.26	1.037	4.71	5.55(−28)		0.121
1300	35.51	1.040	4.80	2.44(−26)		0.106
1400	33.07	1.044	4.88	6.20(−25)		0.094
1500	30.89	1.047	4.98	1.03(−23)		0.083
1600	28.93	1.050	5.08	1.18(−22)		0.073
1700	27.16	1.053	5.17	1.01(−21)		0.065
1800	25.56	1.056	5.26	6.79(−21)		0.058
1900	24.11	1.060	5.34	3.71(−20)		0.052
2000	22.79	1.063	5.42	1.70(−19)		0.047
2100	21.58	1.066	5.50	6.73(−19)		0.043
2200	20.47	1.069	5.57	2.34(−18)	0.052	0.039
2300	19.45	1.073	5.64	7.24(−18)	0.043	0.035
2400	18.51	1.076	5.70	2.03(−17)	0.036	0.032
2500	17.65	1.079	5.76	5.23(−17)	0.030	0.029
2600	16.84	1.082	5.82	1.25(−16)	0.026	0.027
2700	16.10	1.086	5.87	2.78(−16)	0.023	0.025
3000	14.22	1.096	6.05	2.21(−15)	0.017	0.019
3400	12.21	1.109	6.30	1.92(−14)	0.012	0.014

[a] $E_0^0 = 117.603$ kcal mol^{-1} from [16].
[b] $F_{anh} = 2.37$ from [19].
[c] H_2O frequencies are 3651.1, 1594.7, and 3755.9 cm^{-1} from [19].
[d] $K_{eq} = 2.209 \times 10^{24}\ T^{0.1879}\ \exp(-59608.8\ K/T)$ molecules cm^{-3} from [16] over the 300–3400 K range (within ±8%), and $k_{0,rec}^{sc} = k_0^{sc}/K_{eq}$.
[e] Lennard–Jones (LJ) collision rates for H_2O–Kr using the method of [20].
[f] In units, cm^3 molecule^{-1} s^{-1}.
[g] Parentheses denotes the power of 10.
[h] Value from [23].
[i] Calculated values of β_c (see text).

In order to explain the data with H_2O as bath gas, we have simply calibrated Eq. (3) to give $k_{1,H_2O} = 20k_{1,Kr}$ at ∼3000 K in accordance with the data of Homer and Hurle [3]. With the assumption of an enhanced collision cross-section for a dipole–dipole interaction, suggesting a T-independent Z_{LJ} of $\sim 1.5 \times 10^{-9}$ cm^3 molecule^{-1} s^{-1}, the derived β_c value at 3000 K is 0.154. This in turn implies an energy transfer parameter of $\Delta E_{down} = 1479$ cm^{-1} for H_2O as the collision partner. Presuming that this energy transfer parameter is appropriate for all temperatures, the derived β_c's then vary smoothly from 0.766 to 0.130 between 300 and 3400 K. The dissociation rate constants with H_2O as bath gas can then be represented by the three-parameter expression

$$k_{1,H_2O} = 1.671 \times 10^2\ T^{-2.440} \exp(-60475\ K/T)\ \text{cm}^3\ \text{molecule}^{-1}\ \text{s}^{-1} \quad (5)$$

The ratio of Eqs. (5) to (4) varies smoothly from 6.7 to 22.2 over the 300–3400 K T-range. Within experimental error, this is consistent with the existing data for the water effect [3,17]. Equation (5) transformed with equilibrium constants to give k_{-1,H_2O} is also shown in the third-order plot, Fig. 5 as the dashed line.

Estimates of relative collision efficiencies for other bath gases have been made for $k_{-1,M}$ by a number

of researchers [17,23–29]; however, there is no clear consensus on the relative effects. We note that relative values determined recently in the work from this laboratory [18] on $H + O_2 + M$ agree well with the inferences of Zellner et al. [23] on the $H + OH + M$ reaction. Presuming our relative effects for He, Ne, Ar, Kr, H_2, N_2, O_2, CH_4, and H_2O (1.1, 0.75, 1.0, 0.95, 3.0, 2.0, 1.5, 7, and 24, respectively, in [18]) are appropriate for this reaction at flame temperatures, $k_{-1,M}$ (and $k_{1,M} = k_{-1,M}K_{eq}$) can be determined as demonstrated by Homer and Hurle [3]; i.e., $k_{1,M} = k_{1,Ar}[\sum_{i=1}^{n} \gamma_i [M]_i / \sum_{i=1}^{n} [M]_i]$, where $[M]_i$'s and γ_i's are absolute concentrations of the various species in the reactive medium and the relative efficiencies, respectively. The derived values for $k_{1,M}$ can then be used along with high-pressure limits to assess the pressure dependence using the usual Troe factorization methods [19,21,22]. If large amounts of an efficient collider are forming in a reactor (e.g., H_2O), this formulation would require a time-dependent rate constant depending on the extent of reaction. Although we have not considered the efficiency of CO_2, we suggest an intermediate value between N_2 and CH_4 of 4.

The rate constant value from the present Eq. (4) can be compared to the value suggested by Baulch in Ar at $T > 2000$ K. The Baulch value [30] is within $\pm 20\%$ of the present results. Lastly, we note that there is no clear way to take efficient colliders like H_2O into account in existing kinetics codes [31,32]. In fact, β_c measurements for polyatomic colliders are scarce, and more data are clearly needed, particularly when large quantities of polyatomics are being produced as a function of time in practical combustion systems.

Note added in proof: In prior discussions, the important effects of the $OH + H + M$ reactions in flow reactor, ignition delay, and flame speed studies in the H_2/O_2 reaction system, have become apparent, and a new analysis [1] based on the earlier work [2] has now appeared. In this new work it was shown that recent changes in the OH enthalpy of formation and rate constants for $H + O_2 \rightarrow OH + O$ and $H + O_2 + M \rightarrow HO_2 + M$, were sufficient to improve the simulated fits for the flow reactor and ignition delay results. The $OH + H + M$ rate constants affected the fits for only laminar flame speeds. Earlier flame speed predictions based on the results of Baulch et al. [30] were too large suggesting a higher value for $k_{1,Ar} = 3.98 \times 10^{-26}\ T^{-2.0}\ cm^6\ molecule^{-2}\ s^{-1}$ [1]. This value agrees well with the present transformed Eqn. (4) over the T-range, ~800–1500 K, but diverges to twice the present value at 3000 K. We believe that a slightly higher apparent value at high T is quite reasonable depending on the extent of reaction (i.e., the buildup of H_2O product), temperature, and species densities in the various regions of the laminar flames.

[1] Li, J.; Zhao, Z.; Kazakov, A.; Dryer, F. L. Int. J. Chem. Kinet. 2004, 36, 566–575.
[2] Mueller, M. A.; Kim, T. J.; Yetter, R. A.; Dryer, F. L. Int. J. Chem. Kinet. 1999, 31, 113–125.

BIBLIOGRAPHY

1. Bauer, S. H.; Schott, G. L.; Duff, R. E. J Chem Phys 1958, 28, 1089–1096.
2. Olschewski, H. A.; Troe, J.; Wagner, H. Gg. Proc Combust Inst 1967, 11, 155–161.
3. Homer, J. B.; Hurle, I. R. Proc R Soc London A 1970, 314, 585–598.
4. Bopp, J. M.; Kern, R. D.; Niki, T. J Phys Chem 1978, 82, 1343–1346.
5. Cathro, W. S.; Mackie, J. C. J Chem Soc, Faraday Trans 1 1972, 68, 150–159.
6. Srinivasan, N. K.; Su, M.-C.; Sutherland, J. W.; Michael, J. V. J Phys Chem A 2005, 109, 1857–1863.
7. Michael, J. V. Prog Energy Combust Sci 1992, 18, 327–347.
8. Michael, J. V. In Advances in Chemical Kinetics and Dynamics; Barker, J. R. (Ed.); JAI Press: Greenwich, CT, 1992; Vol. 1, pp. 47–112, for original references.
9. Michael, J. V.; Sutherland, J. W. Int J Chem Kinet 1986, 18, 409–436.
10. Michael, J. V. J Chem Phys 1989, 90, 189–198.
11. Michael, J. V.; Fisher, J. R. In Seventeenth International Symposium on Shock Waves and Shock Tubes; Kim, Y. W. (Ed.); AIP Conference Proceedings 208, American Institute of Physics: New York, 1990; pp. 210–215.
12. Su, M.-C.; Kumaran, S. S.; Lim, K. P.; Michael, J. V. Rev Sci Inst 1995, 66, 4649–4654.
13. Su, M.-C.; Kumaran, S. S.; Lim, K. P.; Michael, J. V.; Wagner, A. F.; Harding, L. B.; Fang, D. C. J Phys Chem A 2002, 106, 8261–8270.
14. Su, M.-C.; Kumaran, S. S.; Lim, K. P.; Michael, J. V.; Wagner, A. F.; Dixon, D. A.; Kiefer, J. H.; DiFelice, J. J Phys Chem 1996, 100, 15827–15833.
15. Michael, J. V.; Sutherland, J. W.; Harding, L. B.; Wagner, A. F. Proc Combust Inst 2000, 28, 1471–1478.
16. (a) Ruscic, B. Private communication of results based on Active Thermochemical Tables v. 1.25 operating on the Core (Argonne) Thermochemical Network v. 1.045, for OH and H_2O, April 2005; (b) Ruscic, B.; Pinzon, R. E.; Morton, M. L.; von Laszevski, G.; Bittner, S. J.; Nijsure, S. G.; Amin, K. A.; Minkoff, M.; Wagner, A. F. J Phys Chem A 2004, 108, 9979–9997.
17. Getzinger, R. W.; Blair, L. S. Combust Flame 1969, 13, 271–284.
18. Michael, J. V.; Su, M.-C.; Sutherland, J. W.; Carroll, J. J.; Wagner, A. F. J Phys Chem A 2002, 106, 5297–5313.
19. Troe, J. J Chem Phys 1977, 66, 4758–4775; J Phys Chem 1979, 83, 114–126.

20. Cambi, R.; Cappelletti, D.; Liuti, G.; Pirani, F. J Chem Phys 1991, 95, 1852–1861.
21. Troe, J. Ber Bunsenges Phys Chem 1983, 87, 161–169.
22. Gilbert, R. G.; Luther, K.; Troe, J. Ber Bunsenges Phys Chem 1983, 87, 169–177.
23. Zellner, R.; Erler, K.; Field, D. Proc Combust Inst 1977, 16, 939–948.
24. Getzinger, R. W. Proc Combust Inst 1967, 11, 117–124.
25. Halstead, C. J.; Jenkins, D. R. Combust Flame 1970, 14, 321–324.
26. Gay, A.; Pratt, N. H. Proc Int Symp Shock Tubes Waves 1971, 8, 39.
27. Oldenberg, O.; Rieke, F. F. J Chem Phys 1939, 7, 485–492.
28. Black, G.; Porter, G. Proc R Soc London A 1961, 266, 185–197.
29. Rosenfeld, J. L. J.; Sugden, T. M. Combust Flame 1964, 8, 44–50.
30. Baulch, D. L.; Cobos, C. J.; Cox, R. A.; Esser, C.; Frank, P.; Just, Th.; Kerr, J. A.; Pilling, M. J.; Troe, J.; Walker, R. W.; Warnatz, J. J Phys Chem, Ref Data 1992, 21, 411–429.
31. http://www.me.berkeley.edu/gri_mech-3.0/.
32. http://chem.leeds.ac.uk/combustion/combustion.html-1.5/.